

RESEARCH ARTICLE

# An Improved Model for the hTERT Promoter Quadruplex

Jonathan B. Chaires\*, John O. Trent, Robert D. Gray, William L. Dean, Robert Buscaglia, Shelia D. Thomas, Donald M. Miller

James Graham Brown Cancer Center, Department of Medicine, University of Louisville, Louisville, Kentucky, United States of America

\*[j.chaires@louisville.edu](mailto:j.chaires@louisville.edu)

## Abstract

Mutations occur at four specific sites in the hTERT promoter in >75% of glioblastomas and melanomas, but the mechanism by which the mutations affect gene expression remains unexplained. We report biophysical computational studies that show that the hTERT promoter sequence forms a novel G-quadruplex structure consisting of three contiguous, stacked parallel quadruplexes. The reported hTERT mutations map to the central quadruplex within this structure, and lead to an alteration of its hydrodynamic properties and stability.



CrossMark  
click for updates

## OPEN ACCESS

**Citation:** Chaires JB, Trent JO, Gray RD, Dean WL, Buscaglia R, et al. (2014) An Improved Model for the hTERT Promoter Quadruplex. PLoS ONE 9(12): e115580. doi:10.1371/journal.pone.0115580

**Editor:** Mark Isalan, Imperial College London, United Kingdom

**Received:** September 26, 2014

**Accepted:** December 1, 2014

**Published:** December 19, 2014

**Copyright:** © 2014 Chaires et al. This is an open-access article distributed under the terms of the [Creative Commons Attribution License](https://creativecommons.org/licenses/by/4.0/), which permits unrestricted use, distribution, and reproduction in any medium, provided the original author and source are credited.

**Data Availability:** The authors confirm that all data underlying the findings are fully available without restriction. All relevant data are within the paper and its Supporting Information files.

**Funding:** This work was supported by NIH grants CA35635 (JBC), GM077422 (JBC & JOT) and 1P30GM106396-01 (DMM) and by the James Graham Brown Foundation. The funders had no role in study design, data collection and analysis, decision to publish, or preparation of the manuscript.

**Competing Interests:** The authors have declared that no competing interests exist.

## Introduction

Over the past decade, genomic DNA sequencing efforts have revealed the broad mutational landscapes of common human cancers [1]. Despite these advances, mutations in the promoters of cancer genes have not been documented as a common cause of gene dysregulation in cancer. Using whole genome sequencing data, several groups have recently shown that mutations occur at four specific sites in the hTERT promoter [2–4] in >75% of glioblastomas and melanomas. Additionally, the cooperation of BRAF and hTERT mutations was recently reported in aggressive thyroid cancer [5]. Some of these mutations involve cytosine to thymine transitions suggesting that, in the case of melanoma, they may be UV induced. The guanine to adenine mutations create a new binding site for the E-twenty six (ETS) transcription factor, which has been hypothesized to be the mechanism of increased hTERT expression [2, 3].

We noticed that these mutations all occur in a G-rich region of the hTERT promoter which has previously been shown to form quadruplex DNA [6]. We speculated that the occurrence of these mutations could destabilize, or alter the recognition of, quadruplexes formed by this sequence. This would be expected to

abrogate the negative effect of quadruplex formation on the transcriptional activity of the hTERT promoter, allowing increased hTERT expression.

Quadruplex DNA is a four-stranded structure that is stabilized by G-quartets (four guanines which interact via Hoogsteen hydrogen bonding to form a planar tetrad ring [7, 8]). There are more than 370,000 putative quadruplex-forming sequences (QFS) in the human genome, which are disproportionately represented in the promoters of growth regulatory genes [9, 10]. Roughly half of human promoters contain QFS. These sequences can form either intramolecular or intermolecular Hoogsteen hydrogen bonds stabilizing their secondary and tertiary structure [8, 11]. Recent work has provided clear evidence that quadruplex structures exist in both RNA and DNA *in vivo* eukaryotes [12–14]. The QFS in the c-myc [15], c-Myb [16], K-Ras [17], Bcl-2 [18, 19], retinoblastoma [20] and HIF1 $\alpha$  [21] gene promoters are all in important regulatory regions. In the instance of c-myc and hTERT, the molecular function has been characterized and there is clear evidence that quadruplex formation inhibits gene expression, presumably by silencing transcription [6, 22]. Ironically, quadruplex-forming sequences also occur in telomeric DNA [23, 24] helping provide protection for chromosomal ends.

The locations of the reported hTERT promoter mutations are shown in Fig. 1, along with the structure of the hTERT promoter proposed by Palumbo *et. al* [6]. In that structure the reported G to A transitions would be somewhat oddly placed with one in the hairpin loop, one in the duplex stem and one in the antiparallel quadruplex. The effects of these transitions on the stability and function of the proposed structure are by no means clear. We describe here a new detailed model for the hTERT quadruplex structure completely consistent with biophysical data. In the new model, mutations are localized within a single central G-quadruplex. The mutations may alter the stability and molecular recognition of the hTERT quadruplex.

## Materials and Methods

### Oligodeoxynucleotides

Names, sequences and absorption coefficients of the oligonucleotides used in this study are given in Table 1. hTERT (obtained from Oligos Etc.) was dissolved in water at a concentration of 650  $\mu$ M. 1XAV was from IDT, Coralville, IA. The lyophilized, desalted powder was dissolved in 10 mM LiPO<sub>4</sub>, pH 7.0 at a concentration of 2 mM. The stock solutions of both oligonucleotides were stored at 4°C. Solutions for fluorescence polarization studies were prepared at  $\sim$ 1  $\mu$ M concentration in 10 mM tetrabutyl ammonium phosphate, 1 mM EDTA, 200 mM KCl, pH 7.0 (referred to hereafter as tBAP folding buffer), denatured at 90°C in a water bath for 10–15 min, followed by annealing by slowly cooling to room temperature in the bath. Folding to the quadruplex state was checked by recording the CD spectrum of the sample over the wavelength range 340 nm to

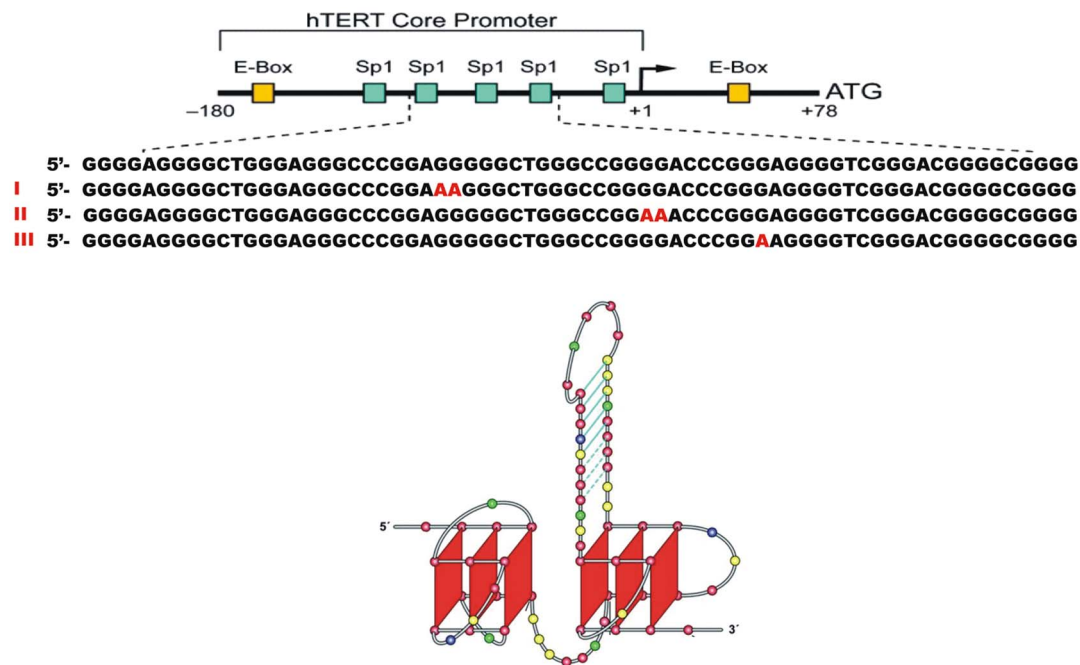


**Fig. 1. The hTERT promoter sequence and proposed structure.** *Top:* Sequence of the hTERT core promoter with the positions of mutations observed in melanomas shown in red. *Bottom:* Previously proposed structure of the hTERT core promoter (5). Adapted with permission from (5).

doi:10.1371/journal.pone.0115580.g001

220 nm and observing a maximum in the CD spectrum at 260 nm and a minimum at 240 nm.

### Reagents

Thiazole orange, whose fluorescence quantum yield increases significantly when bound to DNA [25], was from Sigma Chemical Co. (St. Louis, MO). A stock solution of 250 μM dye was prepared in folding buffer containing 200 mM KCl and 20% sucrose. The final concentrations of the dye and oligonucleotide in the fluorescence polarization experiments was estimated by spectrophotometry with a Jasco V-550 instrument in conjunction with the appropriate absorption coefficient for the DNA along with a value of  $\epsilon_{500 \text{ nm}}$  of  $63 \text{ mM}^{-1} \text{ cm}^{-1}$  for the dye. To ensure a negligible concentration of free dye, polarization experiments were carried out with excess DNA (DNA:dye $\approx$ 3:1).

**Table 1.** Oligodeoxynucleotides used in this study.

Name	Sequence	MW	$\epsilon_{260 \text{ nm}}$ ( $\text{mM}^{-1} \text{ cm}^{-1}$ )
hTERT	5'-GGG GAG GGG CTG GGA GGG CCC GGA GGG GGC TGG GCC GGG GAC CCG GGA GGG GTC GGG ACG GGG CGG GG-3'	21632.8	659.3
1XAV	5'-TGA GGG TGG GTA GGG TGG GTA A-3'	6991.6	228.7

doi:10.1371/journal.pone.0115580.t001

KCl, tetrabutylammonium dihydrogen phosphate, tetrabutylammonium hydroxide and EDTA (acid form) were from Sigma. Sucrose was from Mallinckrodt Chemicals, Phillipsburg, NJ, and  $\text{LiH}_2\text{PO}_4$  and LiOH monohydrate were from Aldrich Chemicals, Milwaukee, WI.

### Circular Dichroism and Thermal Denaturation

Thermal denaturation of quadruplexes was monitored using a Jasco J-810 spectropolarimeter (Jasco Inc., Easton, MD) equipped with a programmable Peltier thermostatted cell holder and a magnetic stirrer. CD spectra were collected using instrumental parameters:  $280 < \lambda < 350$  nm, 1.0 nm step size, 200 nm/min scan rate, 1.0 nm bandwidth, 2 s integration time, with 4 total scans averaged. For melting experiments, samples at 3–4  $\mu\text{M}$  in a 1-cm path length cuvette were equilibrated in the cuvette holder at 4°C prior to starting the melt. Melting experiments were carried out with the thermal parameters: 4°C/min ramp, 0.05°C equilibration with a 60 s delay prior to acquisition. Spectra were corrected by subtracting a solvent blank. Melts were carried out in duplicate on successive days; data presented here are from the second melt. CD data were normalized to molar circular dichroism ( $\Delta\epsilon$ ) based on DNA strand concentration using [equation \(1\)](#)

$$\Delta\epsilon = \theta / (3298.2cl) \quad (1)$$

where  $\theta$  is the CD ellipticity in millidegrees,  $c$  is DNA concentration in mol/L, and  $l$  is the path length in cm.

### Analytical Ultracentrifugation

Sedimentation velocity measurements were carried out in a Beckman Coulter ProteomeLab XL-A analytical ultracentrifuge (Beckman Coulter Inc., Brea, CA) at 20.0°C and at 50,000 rpm in standard 2 sector cells. Data (200 scans collected over a 10 hour centrifugation period) were analyzed using the program Sedfit in the continuous  $c(s)$  mode or by a model assuming discrete, noninteracting species ([www.analyticalultracentrifugation.com](http://www.analyticalultracentrifugation.com)). Buffer density was determined on a Mettler/Par Calculating Density Meter DMA 55A at 20.0°C and buffer viscosity was measured on an Anton Paar Automated Microviscometer AMVn. For the calculation of frictional ratio, 0.55 mL/g was used for partial specific volume and 0.3 g/g was assumed for the amount of water bound. hTERT sequences were dissolved to give a final concentration of 1 mM in tBAP folding buffer, diluted to give an absorbance at 260 nm of 0.5, heated in a boiling water bath for 10 minutes and allowed to cool to room temperature before centrifugation.

### Molecular Dynamics Simulations and HYDROPRO Calculations

Molecular models of G-quadruplex structures were created using the parallel quadruplex structure 1XAV from the Protein Data Bank with manual modification of the loop regions to for the hTERT sequence. Appropriate

coordinating ions were added to the stacked G-tetrads of each model and additional ions were added to neutralize the G-quadruplex structures. The system was solvated in a rectilinear box of TIP3P water molecules with 15 Å buffer. The system was equilibrated using the following protocol: (i) minimize water and ions (1000 steps - 500 steepest descents) holding the DNA fixed (50 kcal/mol/Å), (ii) 50ps MD (heating to 300 K) with 20 ns MD as the production trajectory. A further 10 ns of accelerated MD production trajectory was obtained [26]. Simulations were performed in the isothermal isobaric ensemble ( $P=1\text{atm}$ ,  $T=300\text{K}$ ) using sander and GPU version of pmemd (AMBER 13). Periodic boundary conditions and Particle-Mesh-Ewald algorithms were used. A 2.0 fs time step was used with bonds involving hydrogen atoms frozen using SHAKE. Analysis of the trajectory was performed using the *cpptraj* module of the AmberTools 13 Package. Calculations of hydrodynamic properties were done using the program HYDROPRO 10 [27] using the recommended quadruplex parameters [28] on 5000 snapshots of the accelerated MD trajectory.

### Fluorescence experiments

Fluorescence excitation, emission, and polarization spectra were determined with a Jasco FP-6500 fluorescence spectrophotometer equipped with an ADP-303T Peltier temperature controller and an APH-103 fluorescence polarization unit (Jasco, Inc., Easton, MD). Instrumental settings were:  $\lambda_{\text{ex}}=510\text{ nm}$ ,  $\lambda_{\text{em}}=530\text{ nm}$ , 5 nm emission and excitation bandwidth, 2 s response time. Excitation and emission spectra were corrected by subtraction of a solvent blank.

### Determination of rotational relaxation time

The rotational relaxation time of a particle is defined as the time required for it to rotate through an angle  $\theta$  of  $68.4^\circ$  ( $\cos\theta=1/e$ ). This time depends on the volume  $V$  of the molecule as well as the viscosity  $\eta$  and temperature  $T$  of the medium through the relationship  $\rho=3\eta V/RT$ . The rotational relaxation time  $\rho_0$  for a spherical molecule without bound solvent can be calculated from the relationship  $\rho_0=3\eta M\bar{v}/RT$ , where  $M$  is the molecular weight and  $\bar{v}$  is the partial specific volume (taken as  $0.55\text{ cm}^3/\text{mol}$  for DNA quadruplexes). The ratio  $\rho/\rho_0$  is considered to indicate deviations from a spherical shape and/or hydration of the molecule. The rotational relaxation time as defined above is related to the rotational correlation time  $\phi$  (the time required for a molecule to rotate through 1 radian) by the equation  $\phi=3\rho$  [29].

The rotational relaxation time of a fluorescently labelled molecule can be determined by measuring the degree of fluorescence polarization as a function of viscosity of the solution which can be varied by changing the temperature. Rotational relaxation times for the complexes of hTERT-FL and 1XAV with thiazole orange were determined in tBAP folding buffer with 200 mM KCl and 20% (w/v) sucrose at  $2^\circ\text{C}$  intervals over the temperature range 5 to  $39^\circ\text{C}$ . The

viscosity of the sucrose solution at the experimental temperatures were obtained by interpolation (where necessary) from standard tables<sup>6</sup>.

The data sets were analyzed graphically as described by Montanaro and Sperti [30] using the Perrin equation (Eq. 2) which relates the degree of fluorescence polarization  $P$  to the rotational relaxation time  $\rho$  of the fluorescent particle and  $\tau$ , the lifetime of the excited state:

$$\frac{1}{P} - \frac{1}{3} = \left( \frac{1}{P_0} - \frac{1}{3} \right) \left( 1 + \frac{3\tau}{\rho} \right) \quad (2)$$

$P$  is defined as  $(I_{\parallel} - G \cdot I_{\perp}) / (I_{\parallel} + G \cdot I_{\perp})$ , where  $I_{\perp}$  is the emission intensity with the excitation polarizer at  $90^{\circ}$  (vertical orientation) and the emission polarizer is at  $0^{\circ}$  (horizontal orientation), and  $I_{\parallel}$  is the intensity with both polarizers at  $90^{\circ}$ .  $G$  is a grating correction factor  $= i_{\perp} / i_{\parallel}$  with  $i_{\perp}$  indicating the excitation polarizer is at  $0^{\circ}$  and the emission polarizer is at  $90^{\circ}$ , and  $i_{\parallel}$  indicating that both polarizers are in the  $0^{\circ}$  orientation.  $P_0$  is the intrinsic polarization. The quantity  $(1/P - 1/3)$  is plotted vs.  $T/\eta$  and  $\rho$  is estimated from the slope and intercept estimated by linear regression.

### Determination of fluorescence lifetime

The fluorescence lifetime  $\tau$  for the excited state of thiazole orange bound to hTERT and 1XAV was determined with an ISS K2 Multifrequency Phase Fluorometer (ISS, Champaign, IL). The sample was excited at room temperature with a 468-nm LED and polarizers set at “magic angle” conditions. Emission was measured through a 520-nm band pass filter (Newport Corp.). The instrument was calibrated with fluorescein in 0.1 M NaOH (lifetime=4.0 ns). Phase and amplitude modulation data were analyzed with the ISS program Vinci Beta 1.7 (ISS) to determine lifetimes.

## Results and Discussion

In order to characterize the effects of the observed mutations on the structure and stability of the hTERT core promoter, we initiated several biophysical studies. Fig. 2 shows circular dichroism (CD) spectra for the folded promoter and sequences containing the reported mutations. For the wild-type sequence, the observed CD spectrum is characteristic of a parallel quadruplex structure [31] and is notable for the exceptionally high amplitude of its molar circular dichroism. The observed spectrum is inconsistent with what would be expected for the proposed structure by Palumbo *et. al* [6] (Fig. 1). That structure predicts a spectrum that would be a linear combination of the spectra of a parallel quadruplex, an antiparallel hybrid quadruplex and an 8 bp duplex hairpin. We estimated the predicted spectrum by summing experimental molar circular dichroism spectra for 1XAV (Table 1), a human telomere hybrid quadruplex form and an 8 bp hairpin duplex. The predicted spectrum for that structure, shown in

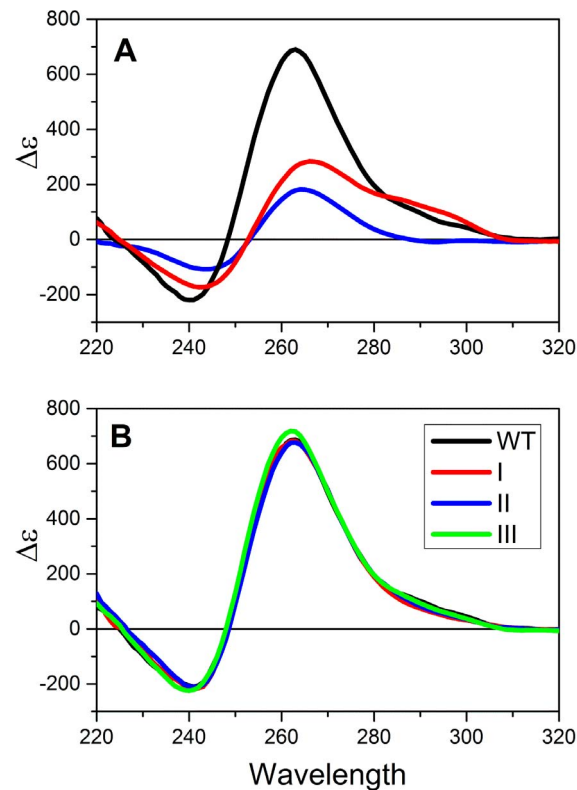


**Fig. 2. Circular dichroism studies of hTERT and mutant sequences.** (A) Molar circular dichroism ( $\Delta\epsilon$ ) of the hTERT promoter sequence in solution (black). The spectrum predicted for the structure shown in Fig. 1 is shown in red. The experimentally observed spectrum for the parallel quadruplex structure formed by the c-myc promoter sequence variant 1XAV is shown in blue. (B). Molar circular dichroism of the folded wild-type and mutant sequences shown in Fig. 1.

doi:10.1371/journal.pone.0115580.g002

red in Fig. 2, differs significantly from the experimentally observed spectrum, especially in the amplitude at 260 nm. For comparison, the spectrum of a three-quartet parallel quadruplex formed by a sequence variant of the c-myc promoter sequence, 1XAV [15], is shown. The shape of that spectrum is similar to the observed hTERT spectrum but the amplitude at 260 nm differs dramatically. The difference in amplitudes can be quantitatively explained if the hTERT structure contains 9 stacked quartets, a structure that might result from the presence of three contiguous parallel quadruplexes that stacked upon one another. Such a structure is a reasonable alternative to the one shown in Fig. 1. Indeed, an hTERT promoter structure consisting of three quadruplexes was previously proposed based on CD spectroscopy and a polymerase stop assay [32] although an actual structure was not proposed.

Fig. 3 shows the results of characterization of the hTERT promoter by sedimentation velocity ultracentrifugation. The distribution ( $c(s)$ ) of sedimentation coefficients is shown and reveals a major species along with a small amount of higher-order species. Analysis of these data using a model of discrete noninteracting species yielded an  $S_{20,w}$  value of  $4.05 \pm 0.04$  for the major (77%)

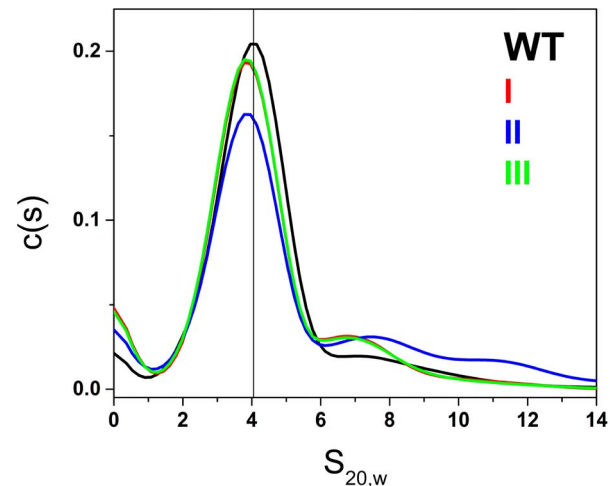


**Fig. 3. Results of sedimentation velocity experiments of hTERT promoter sequences in solution.** The distribution of sedimentation coefficients, corrected for viscosity and temperature, are shown, revealing a major species with  $S_{20,w}$  of  $4.05 \pm 0.04$  for the folded wild-type sequence.  $S_{20,w}$  values for folded mutant sequences are slightly but significantly reduced to 3.5 - 3.6  $S_{20,w}$ .

doi:10.1371/journal.pone.0115580.g003

component. The frictional ratio of this hydrated structure is 1.2, indicative of a nonspherical, asymmetric object [33]. The mass of this species corresponds to the molecular weight of a single strand of the sequence shown in Fig. 1, indicating a folded unimolecular structure. Steady-state fluorescence polarization experiments (S1–S2 Figs.) yielded a rotational relaxation time of  $30.9 \pm 4.1$  ns, compared to a predicted value of 14.6 ns for an equivalent sphere. The ratio of these two values,  $2.1 \pm 0.3$ , again indicates that the folded unimolecular structure is asymmetric.

Minor amounts (14%) of faster sedimenting species (probably aggregates) are seen, along with minor amounts of slower sedimenting material (probably incompletely folded products). We previously determined that human telomere sequences can form structures with three contiguous quadruplexes with  $S_{20,w}$  values of 3.49 and 3.87 for antiparallel and all-parallel conformations, respectively [34]. These values suggest that the hTERT sequence forms a three quadruplex structure of some form, consistent with the conclusion based on CD spectra. A three-dimensional molecular model of mixed quadruplex-duplex structure shown in Fig. 1, optimized with explicitly hydrated molecular dynamics, is predicted to have an  $S_{20,w}$  value of 3.2, significantly lower than experimentally observed value, again suggesting that the model is inconsistent with the observed behavior. For mutated sequences, discrete sedimentation coefficients are reduced to 3.5– $3.6 \pm 0.04$   $S_{20,w}$  (Fig. 3). The differences in  $S_{20,w}$  between the wild-type and mutant sequences are significant ( $p < 0.001$ ) given the precision of sedimentation velocity measurements and as determined by a one-way analysis of variance of the experimental data. The reduced  $S_{20,w}$  values indicate hydrodynamically expanded structures compared to the wild-type sequence. Mutations thus seem to unfavorably affect packing of the multiple quadruplex structures. In addition to the reduction in  $S_{20,w}$  values, mutant sequences show a greater propensity to form

aggregated structures, with a concomitant reduction (by 10–15%) in the amount of the major unimolecular species.

Molecular modeling simulations were used to construct a more realistic detailed model of the structure formed by the hTERT core promoter that is consistent with the biophysical data using computational protocols developed in our laboratory [28]. The three-stacked parallel quadruplex model (Fig. 4) was built using known structures with adjustment of the loop regions to be consistent with Micheli *et al* [32]. The 5'-region is the same as the reported NMR structure for a portion of the hTERT promoter sequence [35]. It is possible to construct a model that has all of the major mutations in the central quadruplex G-quartets. The model was fully stable while running a fully solvated 20 ns molecular dynamics trajectory with no disruption to quadruplex or inter-quadruplex stacking. This was followed by 10 ns of accelerated molecular dynamics to sample more conformational space of the loop regions. Hydropro calculations, using our recent quadruplex optimized calibration protocol [28], on 5,000 snapshots from the accelerate molecular dynamics trajectory revealed a range of  $S_{20,w}$  values of 3.95–4.03, in excellent agreement with what was experimentally observed. The resulting structures are (and have to be) extremely compact to maintain these sedimentation values. This structure is predicted to have a rotation relaxation time of 34.4 ns, in excellent agreement with the experimentally measured value. Several alternate models were explored, but none of these predicted hydrodynamic values that agreed with the experimentally measured values. For example, one alternate model was created that maintained the same three quadruplexes but did not have any inter-quadruplex stacking. The calculated  $S_{20,w}$  was 3.1 for this “beads-on-a-string” parallel structure, far from the experimental value and indicating that noninteracting quadruplex formation alone cannot account for the biophysical data. Similarly, a three-quadruplex structure with antiparallel quadruplex units could not account for the observed biophysical data.

Sedimentation and circular dichroism data are thus entirely consistent with a compact structure in which three parallel quadruplexes are tightly stacked on one another. The complex quadruplex-duplex structure (5) and the multiple “beads-on-a-string” quadruplex structure (25) are inconsistent with our biophysical data.

Surprisingly, the mutations shown in Fig. 1 have little effect on the thermal stability of the hTERT structure (S3A Fig.). Under the ionic conditions used, thermal denaturation is incomplete at 95°C and the melting temperature at the transition midpoint is greater than 90°C. However if the sequence 5'-GGGGCTGGGCCGGGGACCCGGG is used to form a monomeric quadruplex mutations dramatically decrease the thermal stability (S3B Fig.). That sequence would encompass the central quadruplex-forming sequence in the hTERT promoter and readily forms a single parallel quadruplex structure. In the full length hTERT structure allosteric interactions between contiguous quadruplexes apparently mask the destabilizing effects of the mutations. Additionally, we have shown that low-resolution techniques, such as melting, mask the complexity of quadruplex ensemble components [36].

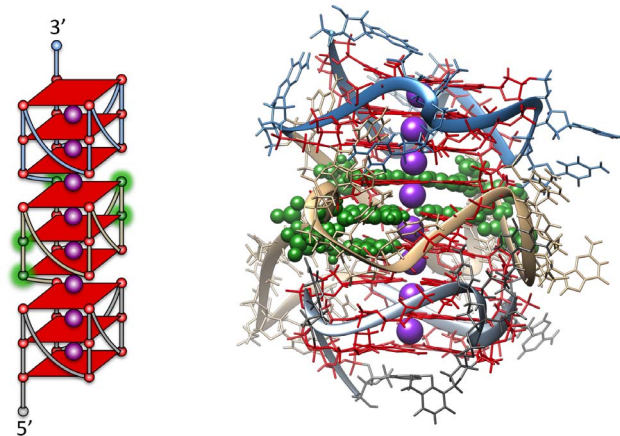


**Fig. 4. Molecular model for the hTERT promoter structure featuring three stacked parallel quadruplexes (right).** The model predicts  $S_{20,w}=4.00\pm 0.1$ , in excellent agreement with the observed value of the wild-type sequence. The sites of reported mutated bases within the central quadruplex are colored in green. A schematic of the structure is shown on the left side, with the sites of mutations highlighted in green.

doi:10.1371/journal.pone.0115580.g004

While the mutations can be accommodated by alternate G-quadruplex formation in the longer sequences (which could account for the similar thermal stability), this would require a reduction to a two-tetrad stacked central quadruplex or by mixed guanine-adenine stacking. However, this would require changes in the connecting and internal loop structures of the central quadruplex, thus lowering the  $S_{20,w}$  value due to longer loops and decreased compactness, as is in fact observed in Fig. 3. Such alterations would affect recognition elements, protein binding and/or stability.

Detailed structural studies on quadruplex forming sequences in promoter regions have been limited to single quadruplex structures and often these shorter sequences are highly manipulated to reduce polymorphism. This study indicates that the longer promoter region QFS may be much more complicated and more biologically contextual. This may well be a general phenomenon as these extended QFS are common in the promoters of proto oncogenes that have not been previously examined in this detail.

More than 90% of human tumors overexpress telomerase, as do rapidly dividing cells such as stem cells and germ cells [37, 38]. The mechanism by which hTERT expression is dysregulated has been largely unknown. The data presented here indicate that the common mutations in the hTERT promoter occur in a quadruplex structure in this region. It is possible, by altering recognition elements and stability of this region, that the “transcriptionally active” duplex DNA structure with the ETS binding site would be favored. Importantly, ETS binding likely helps stabilize the double stranded (transcriptionally active) structure. This loss of quadruplex stability could abrogate the gene silencing effects of quadruplex formation, allowing increased hTERT expression. Because of its ubiquitous overexpression and its critical role in almost all tumors, telomerase is an excellent therapeutic target [39, 40]. The concept of reversing promoter silencing via

mutations that cause quadruplex destabilization is an exciting new paradigm and provides the first plausible rationalization of mutation mediated gene transcription by quadruplex control.

## Supporting Information

**S1 Fig. Representative response curves for phase delay and modulation ratio for determination of fluorescence lifetimes of thiazole orange bound to oligonucleotide 1XAV (panel A) and hTERT (panel B).** The points represent the experimental data and the lines represent the best fit of the data points using the lifetimes and fractional contributions of each to a two-lifetime model. The lower panels show the residuals for each fit. The data were analyzed using the program Vinci Beta 1.7. Experimental conditions: 0.9  $\mu\text{M}$  1XAV, 0.3  $\mu\text{M}$  thiazole orange; 1.4  $\mu\text{M}$  hTERT, 0.4  $\mu\text{M}$  thiazole orange. Determinations were made at room temperature ( $\sim 21^\circ\text{C}$ ). Both samples were in tBAP folding buffer, 200 mM KCl, 20% sucrose, pH 7.0. Lifetimes and fractions determined by non-linear least squares analysis are shown in the figures.

[doi:10.1371/journal.pone.0115580.s001](https://doi.org/10.1371/journal.pone.0115580.s001) (DOCX)

**S2 Fig. Representative Perrin plots showing the dependence of the fluorescence polarization of oligonucleotide-bound thiazole orange on  $T/\eta$ .** Panel A shows data for 0.9  $\mu\text{M}$  1XAV and 0.3  $\mu\text{M}$  thiazole orange. Panel B shows data for 1.4  $\mu\text{M}$  hTERT with 0.4  $\mu\text{M}$  thiazole orange. Experimental conditions were tBAP folding buffer, 200 mM KCl, 20% sucrose, pH 7.0. The temperature was varied from  $5^\circ\text{C}$  to  $39^\circ\text{C}$  in  $2^\circ\text{C}$  intervals. For this particular set of experiments,  $\rho = 8.8$  ns for 1XAV and 31 ns for hTert.

[doi:10.1371/journal.pone.0115580.s002](https://doi.org/10.1371/journal.pone.0115580.s002) (DOCX)

**S3 Fig. Thermal denaturation of (A) the long hTERT sequences shown in [fig. 1](#) and (B) truncated sequences encompassing the central quadruplex region.**

[doi:10.1371/journal.pone.0115580.s003](https://doi.org/10.1371/journal.pone.0115580.s003) (DOCX)

## Author Contributions

Conceived and designed the experiments: JBC JOT RDG WLD RB SDT. Performed the experiments: RDG WLD RB SDT. Analyzed the data: JBC JOT RDG WLD RB. Contributed reagents/materials/analysis tools: JBC JOT DMM RDG WLD. Wrote the paper: JBC DMM DOT RDG WLD.

## References

1. Vogelstein B, Papadopoulos N, Velculescu VE, Zhou S, Diaz LA Jr, et al. (2013) Cancer genome landscapes. *Science* 339: 1546–1558.
2. Huang FW, Hodis E, Xu MJ, Kryukov GV, Chin L, et al. (2013) Highly recurrent TERT promoter mutations in human melanoma. *Science* 339: 957–959.

3. **Horn S, Figl A, Rachakonda PS, Fischer C, Sucker A, et al.** (2013) TERT promoter mutations in familial and sporadic melanoma. *Science* 339: 959–961.
4. **Killela PJ, Reitman ZJ, Jiao Y, Bettegowda C, Agrawal N, et al.** (2013) TERT promoter mutations occur frequently in gliomas and a subset of tumors derived from cells with low rates of self-renewal. *Proc Natl Acad Sci U S A* 110: 6021–6026.
5. **Xing M, Liu R, Liu X, Murugan AK, Zhu G, et al.** (2014) BRAF V600E and TERT Promoter Mutations Cooperatively Identify the Most Aggressive Papillary Thyroid Cancer With Highest Recurrence. *J Clin Oncol* 32: 2718–2726.
6. **Palumbo SL, Ebbinghaus SW, Hurley LH** (2009) Formation of a unique end-to-end stacked pair of G-quadruplexes in the hTERT core promoter with implications for inhibition of telomerase by G-quadruplex-interactive ligands. *J Am Chem Soc* 131: 10878–10891.
7. **Gellert M, Lipsett MN, Davies DR** (1962) Helix formation by guanylic acid. *Proc Natl Acad Sci U S A* 48: 2013–2018.
8. **Burge S, Parkinson GN, Hazel P, Todd AK, Neidle S** (2006) Quadruplex DNA: sequence, topology and structure. *Nucleic Acids Res* 34: 5402–5415.
9. **Todd AK, Johnston M, Neidle S** (2005) Highly prevalent putative quadruplex sequence motifs in human DNA. *Nucleic acids research* 33: 2901–2907.
10. **Huppert JL, Balasubramanian S** (2005) Prevalence of quadruplexes in the human genome. *Nucleic acids research* 33: 2908–2916.
11. **Neidle S, Parkinson GN** (2003) The structure of telomeric DNA. *Curr Opin Struct Biol* 13: 275–283.
12. **Lam EY, Beraldi D, Tannahill D, Balasubramanian S** (2013) G-quadruplex structures are stable and detectable in human genomic DNA. *Nature communications* 4: 1796.
13. **Biffi G, Di Antonio M, Tannahill D, Balasubramanian S** (2014) Visualization and selective chemical targeting of RNA G-quadruplex structures in the cytoplasm of human cells. *Nature chemistry* 6: 75–80.
14. **Xu Y, Komiyama M** (2013) Evidence for G-quadruplex DNA in human cells. *Chembiochem: a European journal of chemical biology* 14: 927–928.
15. **Ambrus A, Chen D, Dai J, Jones RA, Yang D** (2005) Solution structure of the biologically relevant G-quadruplex element in the human c-MYC promoter. Implications for G-quadruplex stabilization. *Biochemistry* 44: 2048–2058.
16. **Palumbo SL, Memmott RM, Uribe DJ, Krotova-Khan Y, Hurley LH, et al.** (2008) A novel G-quadruplex-forming GGA repeat region in the c-myc promoter is a critical regulator of promoter activity. *Nucleic Acids Res.*
17. **Cogoi S, Xodo LE** (2006) G-quadruplex formation within the promoter of the KRAS proto-oncogene and its effect on transcription. *Nucleic Acids Res* 34: 2536–2549.
18. **Dai J, Chen D, Jones RA, Hurley LH, Yang D** (2006) NMR solution structure of the major G-quadruplex structure formed in the human BCL2 promoter region. *Nucleic Acids Res* 34: 5133–5144.
19. **Dai J, Dexheimer TS, Chen D, Carver M, Ambrus A, et al.** (2006) An intramolecular G-quadruplex structure with mixed parallel/antiparallel G-strands formed in the human BCL-2 promoter region in solution. *J Am Chem Soc* 128: 1096–1098.
20. **Murchie AI, Lilley DM** (1992) Retinoblastoma susceptibility genes contain 5' sequences with a high propensity to form guanine-tetrad structures. *Nucleic Acids Res* 20: 49–53.
21. **De Armond R, Wood S, Sun D, Hurley LH, Ebbinghaus SW** (2005) Evidence for the presence of a guanine quadruplex forming region within a polypurine tract of the hypoxia inducible factor 1alpha promoter. *Biochemistry* 44: 16341–16350.
22. **Siddiqui-Jain A, Grand CL, Bearss DJ, Hurley LH** (2002) Direct evidence for a G-quadruplex in a promoter region and its targeting with a small molecule to repress c-MYC transcription. *Proc Natl Acad Sci U S A* 99: 11593–11598.
23. **Kan ZY, Lin Y, Wang F, Zhuang XY, Zhao Y, et al.** (2007) G-quadruplex formation in human telomeric (TTAGGG)<sub>4</sub> sequence with complementary strand in close vicinity under molecularly crowded condition. *Nucleic Acids Res.*

24. **Sundquist WI, Klug A** (1989) Telomeric DNA dimerizes by formation of guanine tetrads between hairpin loops. *Nature* 342: 825–829.
25. **Nygren J, Svanvik N, Kubista M** (1998) The interactions between the fluorescent dye thiazole orange and DNA. *Biopolymers* 46: 39–51.
26. **Pierce LC, Salomon-Ferrer R, Augusto FdOC, McCammon JA, Walker RC** (2012) Routine Access to Millisecond Time Scale Events with Accelerated Molecular Dynamics. *J Chem Theory Comput* 8: 2997–3002.
27. **Ortega A, Amoros D, Garcia de la Torre J** (2011) Prediction of hydrodynamic and other solution properties of rigid proteins from atomic- and residue-level models. *Biophys J* 101: 892–898.
28. **Le HT, Buscaglia R, Dean WL, Chaires JB, Trent JO** (2013) Calculation of hydrodynamic properties for G-quadruplex nucleic acid structures from in silico bead models. *Top Curr Chem* 330: 179–210.
29. **Jameson DM** (2014) *Introduction to Fluorescence*. Boca Raton, FL: CRC Press.
30. **Montanaro L, Sperti S** (1979) Fluorescence polarization of elongation factor 2. *Methods Enzymol* 60: 712–719.
31. **Karsisiotis AI, Hessari NM, Novellino E, Spada GP, Randazzo A, et al.** (2011) Topological characterization of nucleic acid G-quadruplexes by UV absorption and circular dichroism. *Angew Chem Int Ed Engl* 50: 10645–10648.
32. **Micheli E, Martufi M, Cacchione S, De Santis P, Savino M** (2010) Self-organization of G-quadruplex structures in the hTERT core promoter stabilized by polyaminic side chain perylene derivatives. *Biophys Chem* 153: 43–53.
33. **Schuck P** (2000) Size-distribution analysis of macromolecules by sedimentation velocity ultracentrifugation and lamm equation modeling. *Biophys J* 78: 1606–1619.
34. **Petraccone L, Trent JO, Chaires JB** (2008) The tail of the telomere. *J Am Chem Soc* 130: 16530–16532.
35. **Lim KW, Lacroix L, Yue DJ, Lim JK, Lim JM, et al.** (2010) Coexistence of two distinct G-quadruplex conformations in the hTERT promoter. *J Am Chem Soc* 132: 12331–12342.
36. **Dailey MM, Miller MC, Bates PJ, Lane AN, Trent JO** (2010) Resolution and characterization of the structural polymorphism of a single quadruplex-forming sequence. *Nucleic Acids Res* 38: 4877–4888.
37. **Shay JW, Bacchetti S** (1997) A survey of telomerase activity in human cancer. *European journal of cancer* 33: 787–791.
38. **Hiyama E, Hiyama K** (2007) Telomere and telomerase in stem cells. *British journal of cancer* 96: 1020–1024.
39. **Corey DR** (2009) Telomeres and telomerase: from discovery to clinical trials. *Chemistry & biology* 16: 1219–1223.
40. **Shay JW, Keith WN** (2008) Targeting telomerase for cancer therapeutics. *British journal of cancer* 98: 677–683.